Hindawi
Advances in Civil Engineering
Volume 2020, Article ID 3975745, 16 pages
https://doi.org/10.1155/2020/3975745

Research Article

Displacement Characteristics of an Urban Tunnel in Silty Soil by the Shallow Tunnelling Method

Shaobing Zhang,[1] Siyue He,[1] Junling Qiu,[1] Wei Xu,[1] Rodney Sheldon Garnes,[1,2] and Lixin Wang[1,3]

[1]*School of Highway, Chang'an University, Xi'an 710064, China*
[2]*University of the West Indies, Cave Hill Campus, Cave Hill, St. Michael, Wanstead, Barbados*
[3]*China Railway First Survey and Design Institute Group Co Ltd., State Key Laboratory of Rail Transit Engineering Informatization, Xi'an 710043, China*

Correspondence should be addressed to Junling Qiu; junlingqiu@chd.edu.cn and Lixin Wang; 458601714@qq.com

Received 2 May 2019; Revised 31 August 2019; Accepted 5 September 2019; Published 11 February 2020

Academic Editor: Sanjay Nimbalkar

The urban shallow tunnelling process in silty soil is easy to cause large displacement of surface and tunnel. Obviously, if the strata and the tunnel face are not treated by reasonable reinforcement method, instability and collapse phenomenon will be encountered during the tunnel excavation. There are a series of studies on construction methods of shallow tunnels, but these methods have limitations in silty soil. In this study, a comprehensive construction plan of the urban shallow tunnel in silty soil was proposed and applied to a case study in Fuzhou, Fujian Province in South China. The in situ monitoring tests and numerical simulation were employed to address displacement characteristics of surface and tunnel. Results indicated that the urban shallow tunnelling process could achieve good effect by dewatering of silty soil, reinforcing surface by vertical jet grouting piles, and advanced small pipes and circumferential grouting in the tunnel face; surface settlement during dewatering process accounted for about 30% of total surface settlement in silty soil; the excavation of the top heading, the middle, and lower benches had great effect on displacement of surface and tunnel for three-bench seven-step excavation method in silty soil; surface settlement troughs in silty soil were deeper and wider; lock-feet bolts had good effect on restricting horizontal convergence; and ratio of total crown settlement and total horizontal convergence was in range of 1.43~1.59 when b/h was 0.88 in silty soil. The construction plan proposed in this paper is helpful for further study of shallow tunnel tunnelling process in silty soil.

1. Introduction

In recent years, there are more and more urban shallow tunnels in silty soil. Silty soil has characteristics of high compression, high sensitivity, high creep, high water content, low strength, and so on [1, 2]. Many problems need to be considered in construction process of the urban shallow tunnels in silty soil, for example, treatment of groundwater, selection of reinforcement schemes, and controlling of surface settlement [3]. Meanwhile, silty soil is widely distributed in mainland and coastal areas of the world, especially in China, such as Guangzhou, Nanjing, Shanghai, Hangzhou, and Fuzhou [4–6]. The support system of the urban shallow tunnels in silty soil in recent years in China is shown in Table 1. At present, strata reinforcement can also be carried out by cement mixing piles and jet grouting piles; most of advanced supports in the tunnel face are advanced large pipe-sheds, advanced small pipes, and the tunnel face grouting. To improve stability of silty soil shallow tunnels passing through, it is necessary to seek more effective methods to reduce underwater, strengthen stratum and the tunnel face.

Up to now, many studies about shallow tunnelling process have been conducted. Kirsch [7], Chen et al. [8], Oreste and Dias [9], Zhang et al. [10], Vu et al. [11], and Li et al. [12] adopted numerical simulation and theoretical calculation methods to analyze stability of the excavation face of shallow tunnels in soft soil and sand. Following Peck

Table 1: The support system of urban shallow tunnels in silty soil in recent years in China.

Item	Tunnel name	Strata reinforcement	Advanced support
Guangzhou metro line 2	Xiaogang-Jiangnanxi tunnel	—	Advanced small pipes and tunnel face grouting
Nanjing metro	Zhujiang Road station~Gulou station	—	Advanced large pipe-sheds, advanced small pipes and tunnel face grouting
Shanghai metro line 2	Weining station #3 passageway	—	Advanced large pipe-sheds, deep hole grouting in tunnel face
Guangzhou	Jinshazhou tunnel	Cement mixing piles	Advanced large pipe-sheds
Guangzhou metro line 4	Nanyan section	Cement mixing piles	Synchronous grouting
Hangzhou metro line 4	Zizhi tunnel	Jet grouting piles	Advanced small pipes and tunnel face grouting

[13] and Schmidt [14], Wang et al. [15], Pinto and Whittle [16], Dindarloo and Siami-Irdemoosa [17], and Khademian et al. [18] modified Peck formula to calculate surface settlement troughs and predict the maximum surface settlement due to shallow tunnelling process in soft soil. Fang et al. [19], Yang and Huang [20], Ocak [21], and Bian et al. [22] used field tests and theoretical calculation to study large deformation and rock mass pressure in soft rock of shallow tunnels in soft soil. Additionally, Paternesi et al. [23] and Cao et al. [24] employed finite element analysis and field measurement to analyze surface settlement of shallow tunnelling method (STM) for subway station in soft soil. Fetzer et al. [25], Nazari et al. [26], and Bryk [27] carried out laboratory tests and microscopic photographs to analyze the granular characteristics and permeability of silty soil.

According to the previous literature, the explorations on shallow tunnels have concentrated on studying stability of the tunnel face and characteristics of surface settlement and rock mass pressure in soft soil and sand by shield method; there are several researches about STM of subway station in soft soil; there are a few researches about characteristics of silty soil [28]. Meanwhile, most of existing studies are constructed by shield method, and few studies have focused on displacement characteristics of shallow tunnelling process in silty soil by STM. However, STM is often used in the urban shallow tunnels in silty soil, and it is prone to surface cracking and even surface collapse [29], as shown in Figure 1. Hence, this paper retrospects the case study of STM in silty soil of the Hudonglu tunnel in Fuzhou, Fujian Province in South China, compares the in situ monitoring results and numerical results, analyzes displacement characteristics, and summarizes construction method and supporting measures for urban shallow tunnelling process in silty soil.

2. Project Overview

2.1. Presentation. The Hudonglu tunnel locates in Fuzhou, the provincial capital of Fujian province in South China, as shown in Figure 2. It is the main part of Hudonglu engineering and starts from the Hudong road, ends to the two ring road; the total length of the line is about 1900 m, of which tunnel project is about 1650 m, the tunnel is mainly constructed by open excavation method and STM. The tunnel is arranged with two holes and double lanes, east-west, width (b) of tunnel clearance is 9.2 m, and height of tunnel clearance is 6.75 m.

The left tunnel enters shallow tunnel section at ZK0 + 965 and ends at ZK1 + 350; the right tunnel enters shallow tunnel section at YK1 + 060 and ends at YK1 + 340. The left tunnel ZK1 + 180~ZK1 + 350 enters into silty soil, the right tunnel YK1 + 175~YK1 + 340 enters into silty soil, and longitudinal section of the left tunnel is shown in Figure 3. According to the geological survey report of the earlier stage of Hudonglu tunnel, the geological condition and depth of the right tunnel are similar to that of the left tunnel. The tunnel depth (h) of ZK1 + 180~ZK1 + 350 is 7.9 m~11.2 m. The geological characteristics of strata where tunnel passing through are presented as follows:

(1) Filling soil ($Q4^{ml}$): the soil in this layer is dark gray with loose structure and contains a small amount of gravel, organic matter, and biological debris, and particle size is generally 2.00~4.00 mm. This layer is widely distributed, mainly on surface, with a thickness of 0.60~2.5 m.

(2) Clay ($Q4^{al+pl}$): the soil in this layer is light yellow, plasticity, slightly wet, and contains more clay and silty particles, loose to slightly dense, with a thickness of 0.7~8.1 m.

(3) Strong weathered granite ($\gamma_5{}^{2(3)c}$): the soil in this layer is brownish yellow, massive, and short-columnar and has been completely weathered into gravel clay with poor cohesion and disintegration, with a thickness of 8.2~11.7 m.

(4) Medium weathered granite ($\gamma_5{}^{2(3)c}$): the soil in this layer is generally lighter in color and often rendered with dark brown ferromanganese. Most minerals are severely weathered and metamorphosed. Some have become clay minerals. Original rock structure is clear, and weathering degree of rock mass is often uneven, with a thickness of 6.3~15.8 m.

(5) Silty soil ($Q4^{dl+el}$): the soil in this layer is yellow, wet, and contains clay and organic matter, with average water content 56% and the void ratio 1.54, thixotropy

Figure 1: On-site photos of surface collapse and surface cracking. (a) Shanghai metro line 4, (b) Nanjing metro, (c) Guangzhou metro line 5, (d) Hangzhou metro line 1 [29].

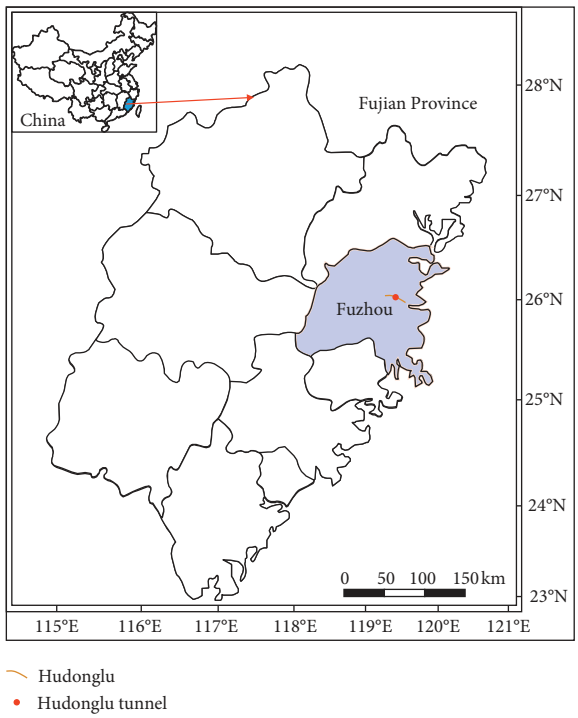

Figure 2: Position of Hudonglu tunnel.

and rheology under saturated condition, with a thickness of 13.2~23.3 m.

(6) Weak weathered granite ($\gamma_5^{2(3)c}$): the soil in this layer is black gray, long-columnar, a few short-columnar, and massive, with well-developed joints and fragmented rock mass, with a thickness of 13.2~24.3 m.

2.2. Construction Scheme. STM is used in Hudonglu tunnel in silty soil. Special construction scheme is adopted for Hudonglu tunnel in silty soil. Well-point dewatering is carried out on surface. Vertical jet grouting piles are used to reinforce strata. Advanced small pipes grouting and circumferential grouting are applied to the tunnel face. Three-bench seven-step excavation method (TSEM) is used for tunnel excavation.

2.2.1. Well-Point Dewatering. Well-point dewatering is a method of lowering groundwater level by setting dewatering wells first and then by pumping equipment, and it is suitable for dewatering in shallow and medium strata within the range of 6~15 m [30, 31]. Well-point dewatering on surface is arranged as in Figure 4, and target dewatering layer is clay and silty soil [32–34]. Dewatering wells enter weak weathered granite 2 m [35–38]. A total of 51 dewatering wells are set up, and the minimum distance between well and tunnel should be determined by actual construction. The minimum distance between two wells should not be less than 14 m; monitoring dewatering wells are set up with 12 ports; and tunnel direction is arranged with distance to 280 m. According to actual situation of in situ monitoring of water level, increase number of dewatering wells if necessary. Because permeability coefficient of clay and silty soil in the site is small, when the effect of dewatering is bad, negative pressure dewatering should be carried out. Construction of

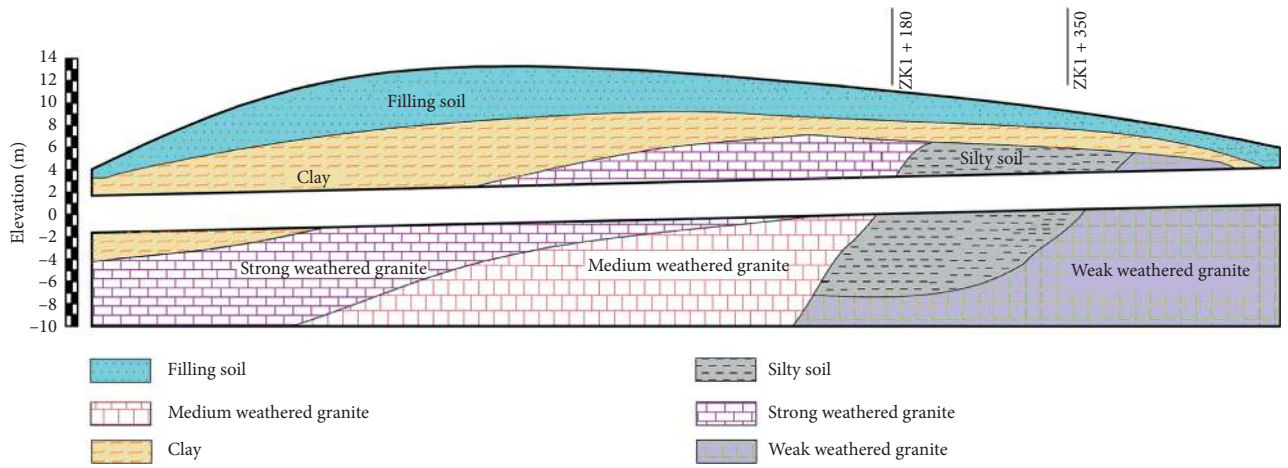

Figure 3: Longitudinal section of the left tunnel.

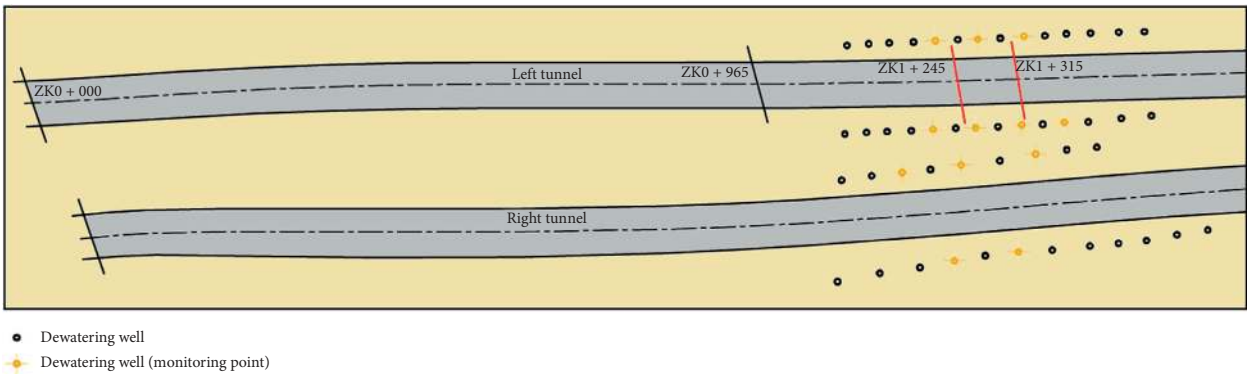

Figure 4: Plane layout of dewatering wells on surface.

negative pressure dewatering wells before tunnel excavation can be adjusted according to the site to avoid buildings on surface.

2.2.2. Surface Reinforcement. Vertical jet grouting piles are selected to reinforce surface of Hudonglu tunnel in silty soil. Through reinforcement ($\Phi = 0.8$ m, $L = 3$ m) of soil on the top of tunnel, crown of tunnel forms a closed shell structure, which can reduce the effect of excavation deformation around tunnel, as shown in Figure 5(a). Both sides of the tunnel use vertical jet grouting piles ($\Phi = 0.8$ m, $L = 8$ m) as curtain for cutting off water, and plane layout of vertical jet grouting piles is arranged as the plum flowers [39–41], as shown in Figure 5(b). There are two rows of piles of curtain for cutting off water on both sides of tunnel; there are 13 rows of piles on the top of the tunnel. Construction technical parameters of vertical jet grouting piles are as follows: they adopt 42.5 R composite Portland cement, water-cement ratio is 0.8~1, air pressure is 0.7 MPa, slurry pressure is 25~30 MPa, lifting speed is 10~15 cm/min, rotation speed is 10 r/min, slurry flow rate is 100 L/min, length of jet lap is 10~15 cm, cement dosage is initially 300~400 kg/m, and cement proportion is controlled 25%~30% [42–44].

2.2.3. Tunnel Support Parameters. Support structure of Hudonglu tunnel in silty soil is shown in Figure 6. Firstly, a single-layer advanced small pipes are used in the tunnel face, diameter of steel pipe is 42 mm, extension length is 2 m, the lapping length of each cycle should be controlled within 1 m, and the scope is 150° of crown of tunnel; at the same time, circumferential grouting in the tunnel face is set with extension length of 4 m. Secondly, steel frame and double-deck steel meshes are constructed; lock-feet bolts (steel, $\Phi = 42$ mm, length = 4.5 m, longitudinal spacing = 1 m) are installed at arch feet to guarantee the stability of the tunnel face, and then 30 cm fiber concrete is sprayed. The deformation allowance between primary support and secondary lining of the tunnel is 5 cm. Finally, 50 cm C35 waterproof concrete is set as secondary lining.

2.2.4. Construction Sequences of TSEM. TSEM is one of the sequential excavation method (SEM), based on the bench cut method, and reserving core soil and staggering excavation from the left to right, which is conducive to stability of the tunnel face [45, 46]. Longitudinal perspective of TSEM is shown in Figure 7 [47–50].

(1) Firstly, the top heading (Stage 1 in Figure 7) is excavated after construction of advanced support, core

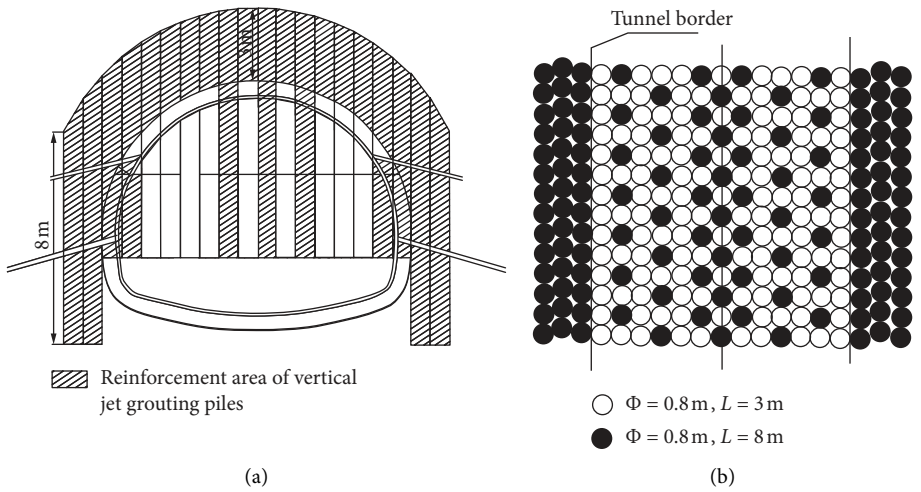

Figure 5: Arrangement of vertical jet grouting piles. (a) Vertical section, (b) horizontal section [39–41].

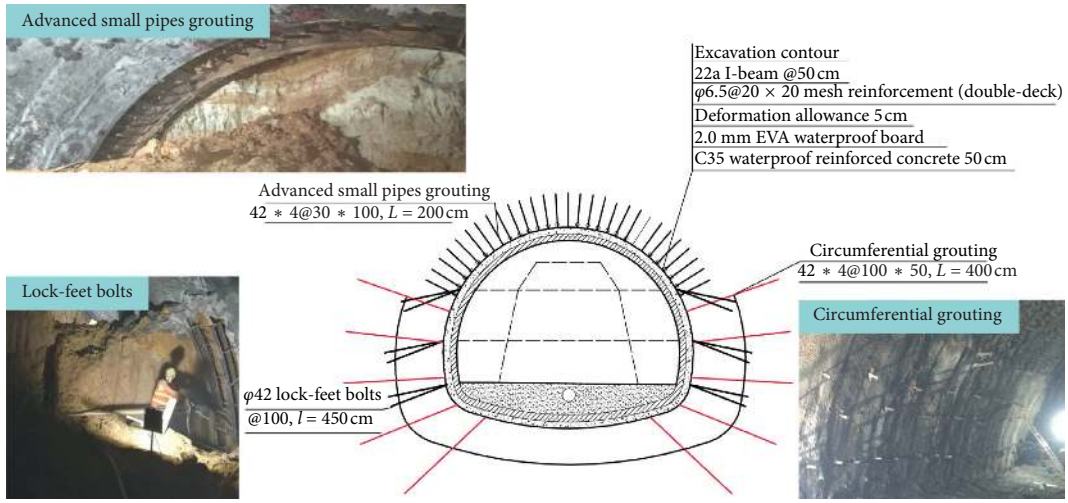

Figure 6: On-site photos and design plan of support structure.

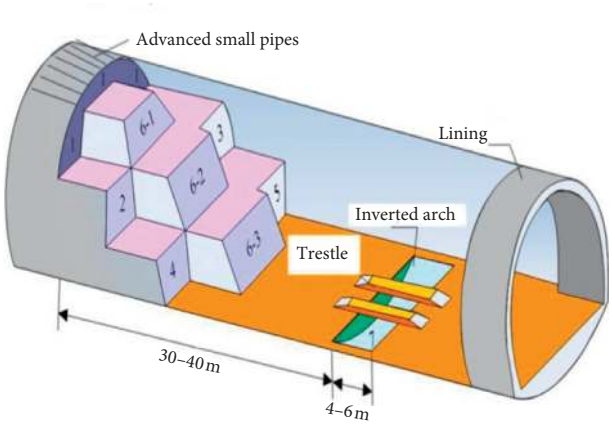

Figure 7: Longitudinal perspective of TSEM [47–50].

soil is reserved, length of core soil is not less than 3 m and width is more than 1/2 width of tunnel excavation, and distance between the top of core soil and the top of the tunnel face is 1.8 m. Excavation distance of the upper bench is 4~6 m, ratio of rise to span is 0.3, excavation step is 0.5~0.6 m, 3~5 cm concrete is sprayed immediately after excavation of the top heading, then steel frame and steel meshes are set up simultaneously. At the height of 30 cm above arch foot of steel frame, lock-feet bolts are set at the edge of 30° on the side of steel frame, and lock-feet bolts are welded firmly into steel frame, then concrete is sprayed to the design thickness (30 cm).

(2) Secondly, the left and right middle benches (Stages 2 and 3 in Figure 7) are, respectively, excavated: excavation step is 1.0~1.2 m, excavation distance is 8~10 m, and the left and right middle bench is stagger 2~3 m. The next construction procedure is the same as the first stage.

(3) Thirdly, the left and right lower benches (Stages 4 and 5 in Figure 7) are, respectively, excavated: excavation step is 1.0~1.2 m, excavation distance is 5~8 m, and the left and right lower bench is stagger

2~3 m. The next construction procedure is the same as the first stage.

(4) Fourthly, core soil (Stages 6-1, 6-2, and 6-3 in Figure 7) is, respectively, excavated. Excavation step is consistent with cyclic step of each bench.

(5) Fifthly, tunnel bottom (Stage 7) is excavated and construction of inverted arch is carried out immediately, and inverted arch is used for each construction of 4~6 m.

(6) Lastly, secondary lining is constructed according to excavation distance.

3. Numerical Simulation

According to geological survey report of the Hudonglu tunnel, the average tunnel depth (h) between ZK1 + 180 and ZK1 + 350 is 10.5 m, and scope of impact radius of the tunnel excavation is considered.

3.1. Calculation Parameters of the Numerical Model

3.1.1. Calculation of Composite Elastic Modulus of Composite Soil. Composite elastic modulus is used to replace the elastic modulus of soil strengthened by vertical jet grouting piles above 3 m of the tunnel. Composite compression modulus of general composite soil can be calculated according to formulas (1) and (2) [51–54]:

$$E_{sp} = mE_p + (1 - m)E_s, \tag{1}$$

$$m = \frac{d^2}{d_e^2}, \tag{2}$$

where E_{sp} is the composite compression modulus of general composite soil, m is the area replacement rate, in equilateral triangle piles, $d_s = 1.05\,s$, s is the pile spacing, E_p is the compression modulus of vertical jet grouting piles, and E_s is the compression modulus of soil between piles.

Foundation soil generally produces elastic-plastic deformation when subjected to loads. Composite elastic modulus reflects modulus of elastic deformation and partial plastic deformation, which is consistent with deformation of foundation soil in general [55–58]. Composite elastic modulus of composite soil can be determined by the following formula :

$$E_0 = \left(1 - \frac{2\mu^2}{1 - \mu}\right)E_{sp}, \tag{3}$$

where E_0 is the composite elastic modulus of composite soil and μ is Poisson's ratio of composite soil (here μ is 0.3).

3.1.2. Conversion of Elastic Modulus of Primary Support. According to principle of simplified compressive rigidity, elastic modulus of medium-sized steel frame with primary support is converted into elastic modulus of shotcrete to simplify the calculation [59–61]. Calculation method is shown in the following formula:

$$E = E_0 + \frac{S_g \times E_g}{S_c}, \tag{4}$$

where E is the elastic modulus of converted shotcrete, E_0 is the elastic modulus of shotcrete, S_g is the sectional area of steel arch, E_g is the elastic modulus of section steel, and S_c is the cross-sectional area of shotcrete.

Composite elastic modulus of composite soil above 3 m of the tunnel can be obtained from formulas (1)–(3), the transformation elastic modulus of primary support can be obtained from formula (4), and the rest parameters are based on geological survey reports and some similar studies, as shown in Table 2 [44, 46].

3.2. Establishment of Numerical Model. Numerical model is based on the MIDAS-GTS (Geotechnical and Tunnel Analysis System) software which is generally used to conduct geotechnical analysis. The layout and sizes of vertical jet grouting piles are referred to Figure 5. The depth of rock mass, the sizes of tunnel, and tunnel support parameters (including advanced support, primary support, and secondary lining) are referred to Figure 6. The construction sequences of TSEM are referred to Figure 7. In addition, the rock mass, composite soil is simulated by solid elements; lock-feet bolts and advanced small pipes are simulated by truss elements; primary support and secondary lining are simulated by shell elements; and vertical jet grouting piles are simulated by beam elements.

In the width direction, calculation range is 120 m, and height of whole model is 47.5 m, and whole numerical model is regular rectangle of 120 m × 50 m × 47.5 m, as shown in Figure 8(a). The support structure of the tunnel is shown in Figure 8(b). The first four construction consequences of STM are shown in Figure 9. According to the actual working conditions, the left tunnel is excavated first, and the right tunnel is excavated later; meanwhile, installing of lock-feet bolts and construction of primary support (Converted shotcrete) are treated as independent construction consequences. Simultaneously, the present three-dimensional model was based on the following assumptions:

(1) All materials in this model are homogeneous, continuous, and isotropous.

(2) Solid elements with elastoplastic materials are subjected to the Mohr–Coulomb yield criterion, and Mohr–Coulomb yield criterion is widely used in similar numerical simulation of tunnel excavation in silty soil; truss elements, beam elements, and shell elements with elastic materials are submitted to the elastic criterion condition.

(3) Soil and pore water are not compressible, and the flow of pore water is subjected to the Darcy law with a constant permeability coefficient k_s.

3.3. Result Analysis

3.3.1. Surface Settlement. Surface settlement characteristics are shown in Figure 10. According to the numerical

Table 2: Mechanical parameters of main strata and supporting materials [44].

Name	Elasticity modulus (MPa)	Poisson's ratio	Bulk density ($kN * m^{-3}$)	Permeability coefficient ($cm * s^{-1}$)	Cohesive force (kPa)	Friction angle (°)
Filling soil	8	0.33	16.5	5×10^{-5}	15.5	9.82
Clay	12	0.30	18.7	1.0×10^{-5}	14.9	12
Silty soil	10	0.38	16.1	1.2×10^{-6}	6.37	15
Weak weathered granite	180	0.28	23	1.2×10^{-3}	800	35
Composite soil	420	0.30	24	1.2×10^{-6}	160	36
Circumferential grouting	360	0.30	24	1.2×10^{-6}	300	30
Converted shotcrete	28000	0.30	24	3.9×10^{-8}	—	—
Secondary lining	31000	0.30	24	1.3×10^{-9}	—	—
Lock-feet bolts	20000	0.30	78.5	—	—	—
Advanced small pipes	20000	0.30	23	—	—	—
Vertical jet grouting piles	1200	0.20	21	—	—	—

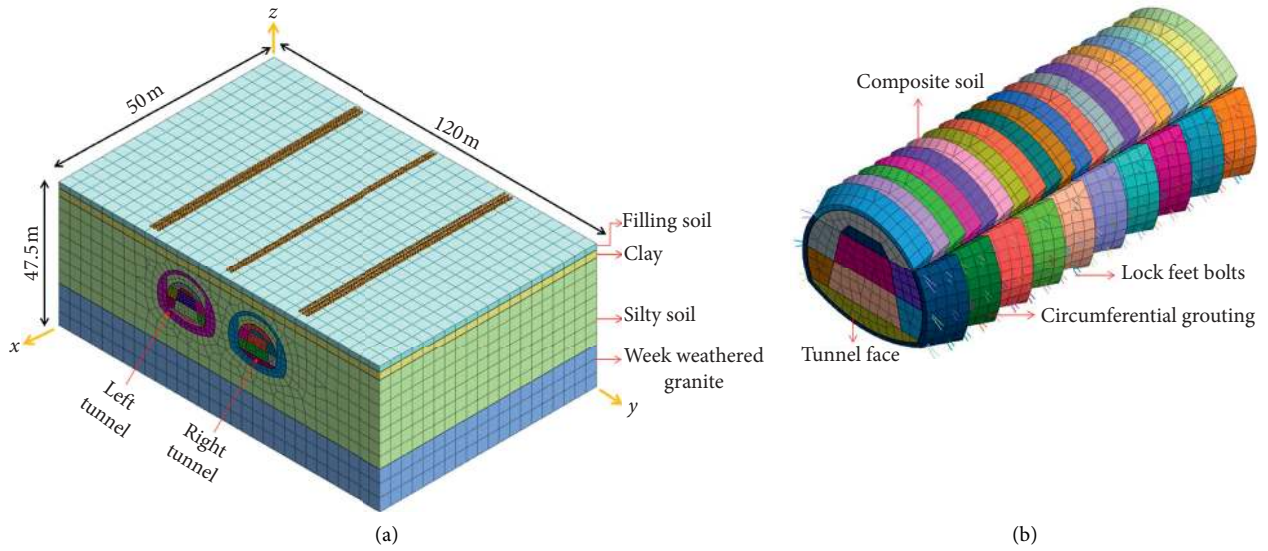

Figure 8: Mesh model. (a) Whole numerical model, (b) Support structure.

simulation, surface settlement characteristics are presented as follows:

(1) The maximum surface settlement is 31.2 mm. When the top heading is excavated, surface settlement change is 4.6 mm. When the middle benches are excavated, surface settlement change is 3.8 mm and 3.2 mm, respectively. When the lower benches are excavated, surface settlement change is 3.5 mm and 2.8 mm, respectively. When primary support is constructed, surface settlement rate decreases rapidly. After filling of inverted arch, surface settlement nearly remains unchanged.

(2) Behind the tunnel face, the surface settlement remains almost unchanged; that is, tunnel excavation has little effect in this region. Within 2b in front of the tunnel face, tunnel excavation has great influence on surface settlement. Within 3b~3.5b in front of the tunnel face, tunnel excavation causes a small amount of uplift on surface.

(3) After middle benches excavation, the maximum surface settlement is 17.2 mm; after lower benches excavation, the maximum surface settlement is 26.8 mm; after filling of inverted arch, the maximum surface settlement is 30.9 mm. The maximum surface settlement occurs above tunnel central line. There is great effect on surface settlement within 1.5b on both sides of tunnel central line, and there is slight uplift between 3b and 3.5b on both sides of tunnel central line.

(4) When double-lane tunnel is excavated, surface settlement shows a double-peak curve, but the curve is not completely symmetrical. After the right tunnel excavation, surface settlement above the left tunnel is slightly affected, which is about 0.2~0.3 mm. Finally, the maximum surface settlement above the left tunnel is 31.2 mm and that of the right tunnel is 29.8 mm.

3.3.2. Crown Settlement. Crown settlement characteristics are shown in Figure 11. According to the numerical simulation, crown settlement characteristics are presented as follows:

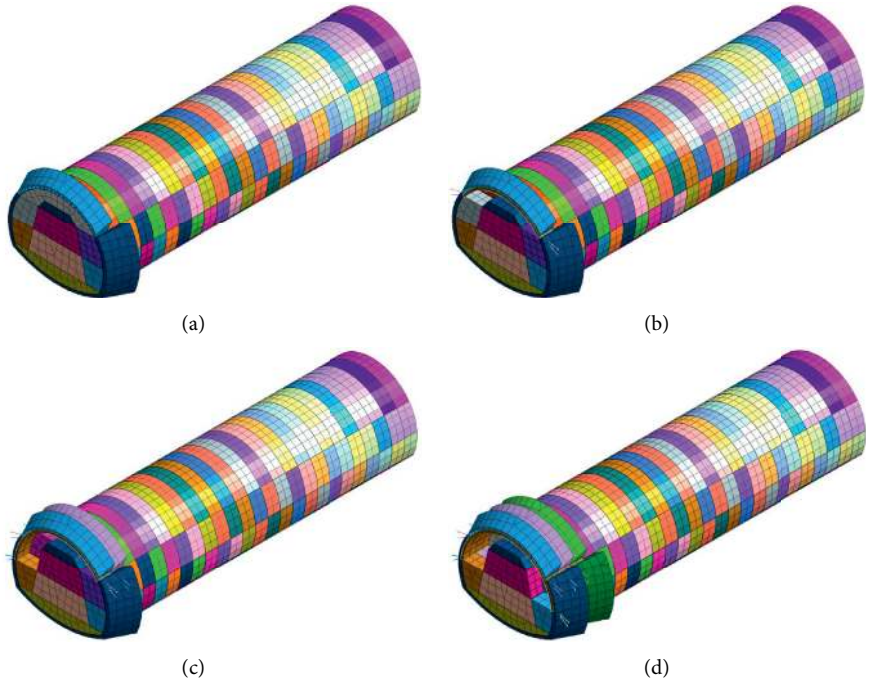

Figure 9: The first four construction consequences of STM: (a) construction of advanced support, (b) Stage 1, (c) Stage 2, and (d) Stage 3.

(1) The maximum crown settlement of tunnel is 74.8 mm. When the top heading is excavated, the crown settlement change is 14.2 mm. Crown settlement change is 1.4 mm after installing of lock-feet bolts. When the middle benches are excavated, crown settlement change is 11.3 mm and 10.2 mm, respectively. Crown settlement change is 1.2 mm and 0.9 mm after installing of lock-feet bolts. When the lower benches are excavated, crown settlement change is 9.8 mm and 7.6 mm, respectively. Crown settlement change is 0.7 mm and 0.4 mm after installing of lock-feet bolts.

(2) Tunnel excavation has a significant effect on crown settlement within 2b in front of the tunnel face. Tunnel excavation has slight effect on crown settlement beyond 3b from the tunnel face. Crown settlement behind the tunnel face is still effected by excavation of the tunnel face, and the effect is about 2~3 m. The farther away depth from crown of the tunnel, the smaller crown settlement of tunnel and approximate to the linear reduction.

(3) It can be seen that after reinforcement of vertical jet grouting piles on the surface, advanced small pipes and circumferential grouting in the tunnel face, the crown settlement and surface settlement converges gradually after the tunnel excavation, and surface and tunnel section reaches stable state. Construction scheme in this paper makes urban shallow tunnelling process in silty soil achieve good effect.

4. In Situ Monitoring Tests

4.1. Monitoring Plan. Monitoring points between ZK1 + 180 and ZK1 + 350 of Hudonglu tunnel in silty soil were shown in Figure 12, and longitudinal distance between two adjacent measuring sections is 5 m. To investigate the behavior of surface settlement, nine measuring points were laid on surface above typical cross sections of tunnel. One measuring point at crown and three measuring lines (arch shoulder, arch waist, and arch foot) at typical cross sections of tunnel were employed to address tunnel displacement [47]. According to the actual situation, there are 30 monitoring sections on surface and 32 monitoring sections of the tunnel.

4.2. In Situ Monitoring Results

4.2.1. Surface Settlement. Table 3 shows statistics of total surface settlement of 30 sections; it could be seen that there were three sections which reached the maximum total surface settlement and that was in range of 7.0~7.5 cm, and there were most sections in which total surface settlement was in range of 6.0~6.5 cm. This phenomenon showed that surface settlement of tunnel construction in silty soil was relatively large and could not be neglected [47, 49], and typical monitoring section was ZK1 + 220 and ZK1 + 337, among which ZK1 + 220 had the maximum total surface settlement, and ZK1 + 337 had the most representative time curves of surface settlement and surface settlement troughs.

Measured time curves of surface settlement of typical section (ZK1 + 220 and ZK1 + 337) are shown in Figure 13. According to the monitoring data, surface settlement characteristics were presented as follows:

(1) Time curves of surface settlement was divided into five periods: period 1, before dewatering, surface settlement changed slowly, about 2.5~3.6 mm; period 2, in dewatering process, surface settlement changed quickly, about 20.9~22.8 mm, the ratio was

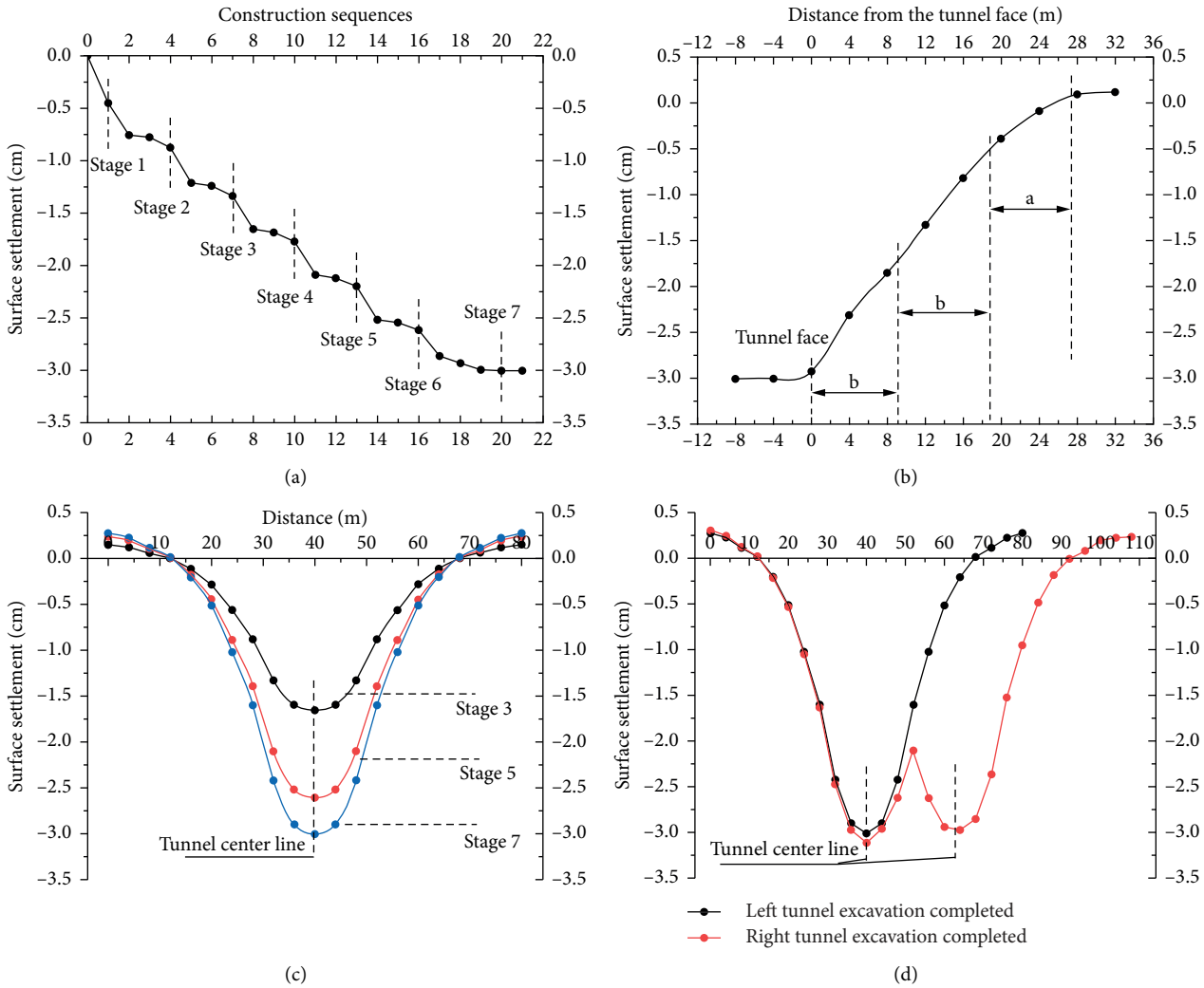

FIGURE 10: Surface settlement characteristics (tunnel face: section $x = 50$ m). (a) Surface settlement with construction sequences, (b) surface settlement with distance from the tunnel face, (c) surface settlement troughs with construction sequences, and (d) whole surface settlement troughs.

30.6~31.1%; period 3, before tunnel construction, surface settlement was basically stable, about 1.5~3.2 mm; period 4, in tunnel construction, surface settlement appeared drastic changed, about 45.2~52.6 mm, the ratio was 61.5%~76.3%; period 5, after tunnel construction, there was some change of surface settlement, about 3.8~8.1 mm, the ratio was 5.1%~11.8%.

(2) Surface settlement changed quickly before stage 5 in tunnel construction, about 28.6~45.2 mm, then surface settlement changed slowly, and the excavation of the rest parts had small effect on surface settlement. There was still some surface settlement after tunnel construction; this may be due to fact that silty soil was not completely stable after completion of secondary lining.

4.2.2. Tunnel Displacement. Tables 4 and 5 show statistics of total tunnel displacement of 32 sections, it could be seen that there were two sections which reached the biggest total crown settlement and that was in range of 9.0~10.0 cm, and there were most sections in which total crown settlement was in the range of 7.0~8.0 cm. Meanwhile, most sections in which total horizontal convergence (arch shoulder) was in the range of 5.0~6.0 cm, and the maximum total horizontal convergence was in the range of 6.0~7.0 cm. Typical monitoring section was ZK1 + 260 and ZK1 + 310, among which ZK1 + 310 had the maximum total crown settlement, and ZK1 + 260 had the most representative time curves of crown settlement and horizontal convergence.

Time curves of tunnel displacement of typical cross sections (ZK1 + 260 and ZK1 + 310) for different construction stages are shown in Figures 14 and 15. According to the monitoring data, tunnel displacement characteristics were presented as follows:

(1) After excavation of the top heading, the crown settlement rate of two sections reached the maximum, about 8.9 mm/d and 9.4 mm/d. After excavation of the lower benches, the crown settlement

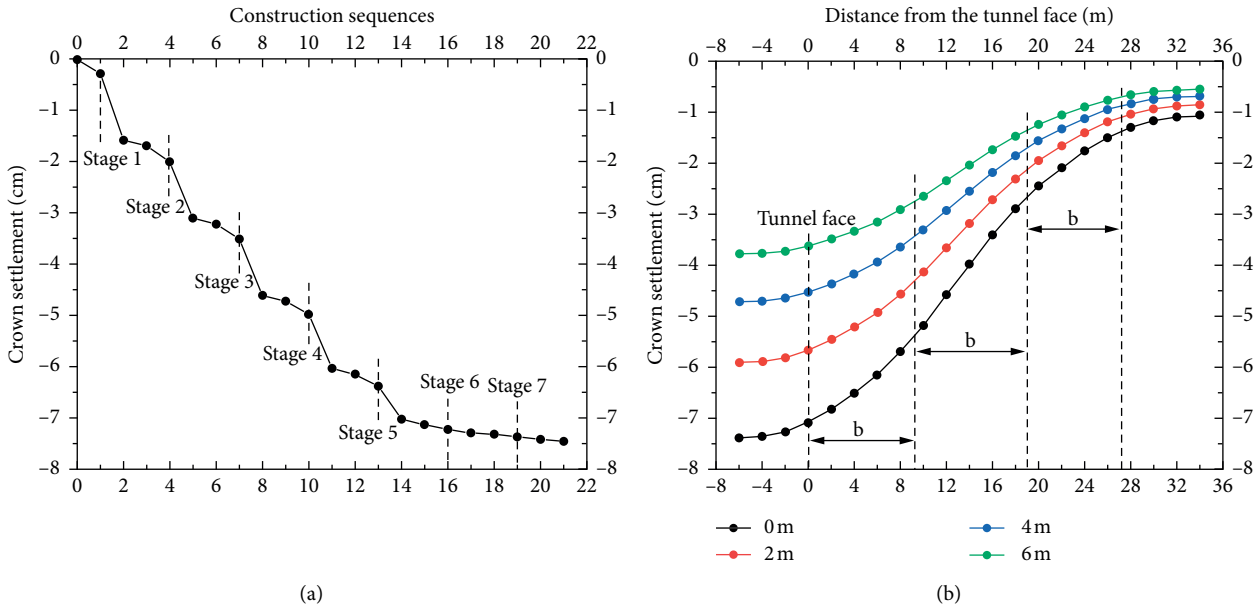

Figure 11: Characteristics of crown settlement of tunnel (tunnel face: section $x = 50$ m). Crown settlement with (a) construction sequences and (b) distance from the tunnel face.

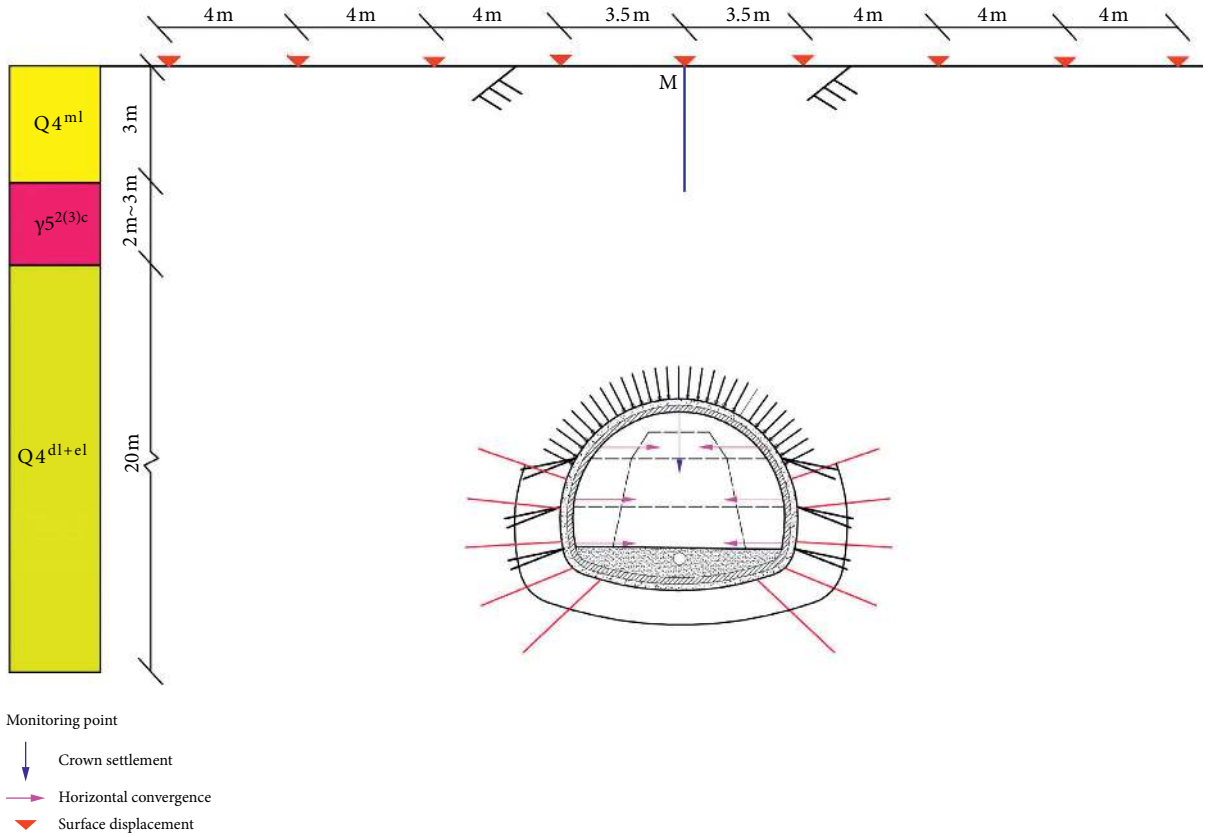

Figure 12: Layout of measuring points [47].

rate of two sections was 4.2 mm/d and 5.0 mm/d; the crown settlement accounted for 84.5%~84.9% of total crown settlement.

(2) The total horizontal convergence of arch shoulder is bigger than arch waist and arch feet. The maximum total crown settlement reached 82.8 mm~99.8 mm.

Table 3: Statistics of total surface settlement (30 sections).

Total surface settlement (cm)					
5.5~6.0	6.0~6.5	6.5~7.0	7.0~7.5	Maximum	Average
6	12	9	3	7.35	6.56

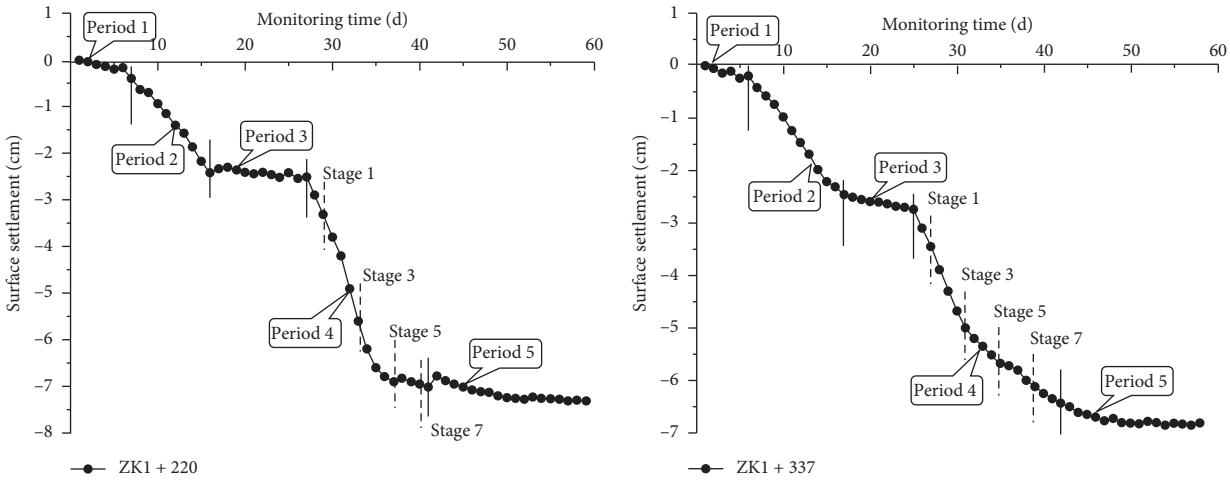

(a) (b)

Figure 13: Measured time curves of surface settlement of section: (a) ZK1 + 220; (b) ZK1 + 337.

Table 4: Statistics of total crown settlement (32 sections).

Total crown settlement (cm)							
5.0~6.0	6.0~7.0	7.0~8.0	8.0~9.0	9.0~10.0	10.0~11.0	Maximum	Average
0	5	16	9	2	0	9.98	8.53

Table 5: Statistics of total horizontal convergence (32 sections).

Position	Total horizontal convergence (cm)								
	1.0~2.0	2.0~3.0	3.0~4.0	4.0~5.0	5.0~6.0	6.0~7.0	8.0~9.0	Maximum	Average
Arch shoulder	0	0	0	7	22	3	0	6.38	5.86
Arch waist	0	6	19	5	2	0	0	5.42	3.68
Arch foot	4	16	10	2	0	0	0	4.36	2.86

The maximum total horizontal convergence reached 57.9 mm~63.3 mm. This showed tunnel excavation had greater effect on crown settlement than horizontal convergence in silty soil section.

(3) Due to the lower strength and higher compression of silty soil, the maximum horizontal convergence rate of arch foot was relatively large. After installing lock-feet bolts, horizontal convergence decreased rapidly, which showed that lock-feet bolts had good effect on reducing horizontal convergence for shallow tunnel in silty soil.

(4) Crown settlement rate and horizontal convergence rate of tunnel decreased with monitoring time. The ratio of the maximum total crown settlement and total horizontal convergence was in the range 1.43~1.59 in silty soil section. There was still some tunnel displacement after excavation of inverted arch, about 1.1~3.5 mm.

4.3. Comparison of Numerical Simulation and In Situ Monitoring Results. Comparison of numerical simulation and in situ monitoring results are shown in Figure 16, and the measured surface settlement is induced by tunnel excavation. Monitoring results of surface settlement and tunnel displacement are slightly larger than those of numerical results, but the laws they reveal are similar. Surface settlement concentrates within 1.5b of the tunnel central line, and the measured maximum surface settlement is in the range of 3.0~4.0 cm. Crown settlement is mainly caused by benches excavation of tunnel; the measured maximum crown settlement is in the range of 8~11 cm. Both displacement of surface and tunnel are at a controllable and secure level.

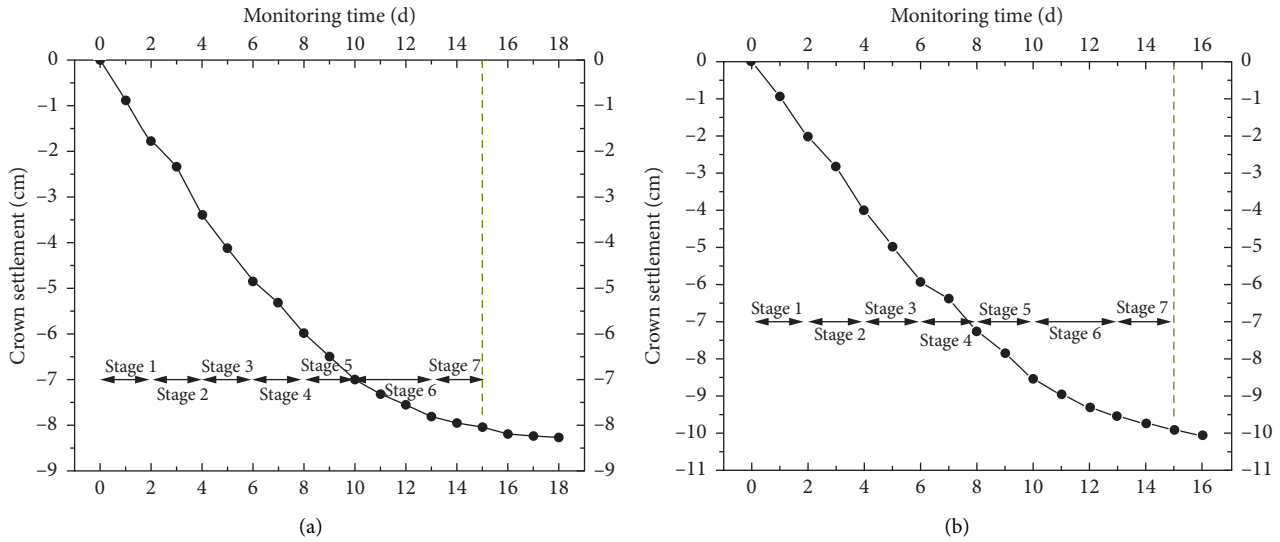

Figure 14: Measured crown settlement-time curves of section: (a) ZK1 + 260; (b) ZK1 + 310.

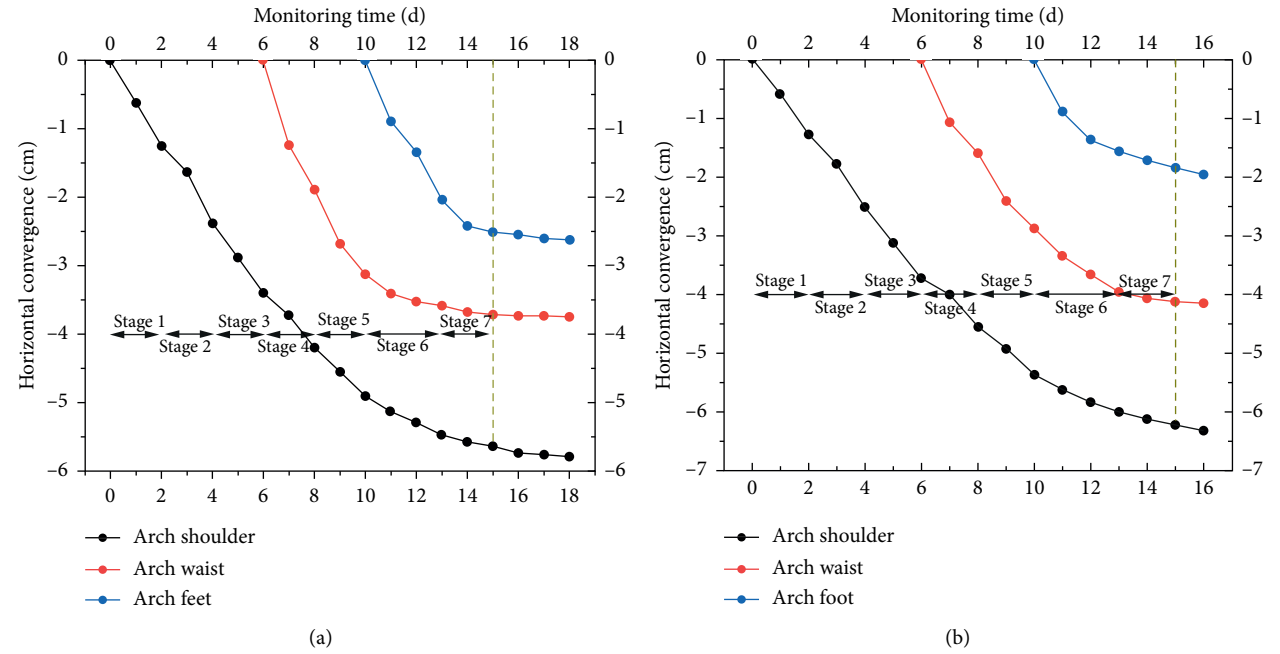

Figure 15: Measured horizontal convergence-time curves of section: (a) ZK1 + 260; (b) ZK1 + 310.

5. Discussions

According to a large number of monitoring data of surface settlement during metro construction, Peck [13] used the "Gauss distribution curve" to fit it and proposed the Peck formula, as shown in formulas (5) and (6). Later, a large number of studies have revised the Peck formula, and it is found that the Peck formula is widely used in predicting surface settlement during metro and shallow tunnel construction [14–18]. In this paper, we make statistics on construction methods and support methods of urban shallow tunnels in silty soil in recent years in China, as shown in Table 1; meanwhile, we calculate the Peck formula parameters of surface settlement troughs of these tunnels, as shown in Table 6. After reasonable strata dewatering, reinforcement of surface, and the tunnel face, the construction of urban shallow tunnel in silty soil by STM can achieve the similar ground loss and small surface settlement as that by shield method, and good construction results have been achieved:

$$S_{\max} = \frac{V_1}{\sqrt{2\pi} i}, \tag{5}$$

$$i = \frac{h + r}{\sqrt{2\pi} \tan\left(45^\circ - (\varphi/2)\right)}, \tag{6}$$

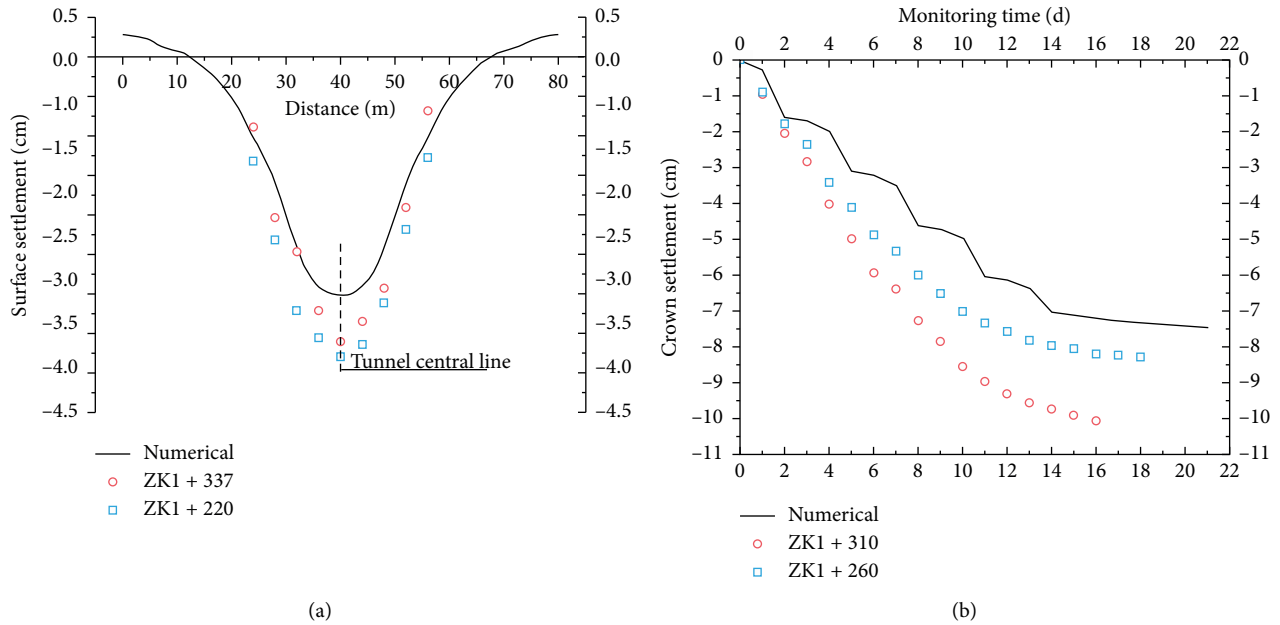

Figure 16: Comparison of numerical simulation and in situ monitoring results: (a) surface settlement; (b) crown settlement.

Table 6: The Peck formula parameters of surface settlement troughs of urban shallow tunnels in silty soil in recent years in China.

Tunnel name	Construction method	Maximum surface settlement (cm)	Trough width parameter (m)	Ground loss (m^3/m)
Xiaogang-Jiangnanxi tunnel	Shield method	3.82	6.34	0.61
Zhujiang Road station~Gulou station	Ring excavation reserving core soil method	3.99	5.91	0.59
Weining station #3 passageway	Bench cut method	5.26	6.67	0.88
Jinshazhou tunnel	CRD	4.12	10.28	1.06
Nanyan section	Shield method	3.52	15.81	1.39
Zizhi tunnel	CRD	10.6	10.35	2.74
Hudonglu tunnel (case study)	TSEM	3.82	8.15	0.78

where S_{max} is the maximum surface settlement, V_1 is the ground loss, i is the trough width parameter, h is the tunnel depth, r is the radius of shield or equivalent radius of tunnel, and φ is the internal friction angle of soil.

Generally, the urban shallow tunnel construction in silty soil is an urgent problem to be solved in tunnel construction in coastal areas. Many studies on tunnel construction in silty soil have proved the difficulty and complexity of the problem [23, 24]. However, there are few studies on urban shallow tunnel construction by STM. In this study, we put forward a comprehensive construction plan for urban shallow tunnel in silty soil by STM and investigate the effect by numerical simulation and in situ monitoring. We found that change regulation of displacement of surface and tunnel, and both of them met requirements of safety and environment during tunnel construction. Our work extended construction method of urban shallow tunnel in silty soil, and it can provide reference for similar projects in the future.

6. Conclusions

This article combines an urban shallow tunnel in silty soil by STM and compares the in situ monitoring results and the FEM results. It can provide new insights into urban shallow tunnel construction in silty soil. The main conclusions are as follows:

(1) For urban shallow tunnel passing through silty soil, a comprehensive construction plan of the well-point dewatering, surface reinforcement with vertical jet grouting piles, advance small pipes and circumferential grouting in the tunnel face, and TSEM can achieve better results, and displacement of surface and tunnel are both controllable.

(2) Numerical results show that surface settlement finally forms settlement troughs; tunnel excavation has obvious influence on surface settlement within 2b in front of the tunnel face; tunnel excavation has

great influence on surface settlement within 1.5b on both sides of the tunnel central line; meanwhile, there are slight uplifts on surface within 3b~3.5b along the tunnel central line.

(3) Comparing in situ monitoring results and numerical results, excavation of the top heading, the middle, and the lower benches have great influence on displacement of surface and tunnel, while excavation of core soil has little effect for TSEM in silty soil; lock-feet bolts have great effect on reducing horizontal convergence. After filling of inverted arch, construction of second lining should be carried out in time.

(4) Both of numerical simulation and in situ monitoring show that silty soil has good elastic characteristics. Surface settlement caused by dewatering process in silty soil accounts for about 30% of total surface settlement in silty soil. The urban shallow tunnel in silty soil by STM could achieve similar construction effect with shield tunnel, including ground loss and surface settlement.

Data Availability

The data used to support the findings of this study are available from the corresponding author upon request.

Conflicts of Interest

The authors declare that they have no conflicts of interest.

Acknowledgments

This work was financially supported by the Fundamental Research Funds for the Central Universities, CHD (Nos. 300102219723, 300102219716, and 300102219711) and National Key R&D Program of China (No. 2017YFC0805306).

References

[1] E. F. Salmi, M. Nazem, and A. Giacomini, "A numerical investigation of sinkhole subsidence development over shallow excavations in tectonised weak rocks: the dolaei tunnel's excavation case," *Geotechnical and Geological Engineering*, vol. 35, no. 4, pp. 1685–1716, 2017.

[2] M. M. Hasan, M. R. Islam, and R. A. Tarefder, "Characterization of subgrade soil mixed with recycled asphalt pavement," *Journal of Traffic and Transportation Engineering (English Edition)*, vol. 3, pp. 57–64, 2018.

[3] N. H. Arash, F. Hadi, and K. Homayoon, "A comparative study on evaluation of steady-state groundwater inflow into a circular shallow tunnel," *Tunnelling and Underground Space Technology*, vol. 73, pp. 15–25, 2018.

[4] K. Wu, Z. S. Shao, S. Qin, and B. X. Li, "Determination of deformation mechanism and countermeasures in silty clay tunnel," *Journal of Performance of Constructed Facilities*, vol. 34, no. 1, Article ID 04019095, 2020.

[5] W. C. Cheng, G. Li, N. Liu, J. Xu, and S. Horpibulsuk, "Recent massive incidents for subway construction in soft alluvial deposits of Taiwan: a review," *Tunnelling and Underground Space Technology*, vol. 96, Article ID 103178, 2020.

[6] K. Wu and Z. S. Shao, "Visco-elastic analysis on the effect of flexible layer on mechanical behavior of tunnels," *International Journal of Applied Mechanics*, vol. 2019, Article ID 1950027, 21 pages, 2019.

[7] A. Kirsch, "Experimental investigation of the face stability of shallow tunnels in sand," *ACTA Geotechnica*, vol. 5, no. 1, pp. 43–62, 2010.

[8] R. P. Chen, L. J. Tang, D. S. Ling, and Y. M. Chen, "Face stability analysis of shallow shield tunnels in dry sandy ground using the discrete element method," *Computers and Geotechnics*, vol. 38, no. 2, pp. 187–195, 2011.

[9] P. P. Oreste and D. Dias, "Stabilisation of the excavation face in shallow tunnels using fibreglass dowels," *Rock Mechanics and Rock Engineering*, vol. 45, no. 4, pp. 499–517, 2012.

[10] C. Zhang, K. Han, and D. Zhang, "Face stability analysis of shallow circular tunnels in cohesive-frictional soils," *Tunnelling and Underground Space Technology*, vol. 50, pp. 345–357, 2015.

[11] M. N. Vu, W. Broere, and J. W. Bosch, "Structural analysis for shallow tunnels in soft soils," *International Journal of Geomechanics*, vol. 17, no. 8, 2017.

[12] P. Li, F. Wang, C. Zhang, and Z. Li, "Face stability analysis of a shallow tunnel in the saturated and multilayered soils in short-term condition," *Computers and Geotechnics*, vol. 107, pp. 25–35, 2019.

[13] R. P. Peck, "Deep excavation and tunneling in soft ground," in *Proceedings of 7th International Conference On Soil Mechanics And Foundation Engineering*, pp. 225–290, Mexico City, Mexico, 1969.

[14] B. Schmidt, "A method of estimating surface settlement above tunnels constructed in soft ground," *Canadian Geotechnical Journal*, vol. 20, pp. 11–22, 1969.

[15] Z. Wang, R. C. K. Wong, S. Li, and L. Qiao, "Finite element analysis of long-term surface settlement above a shallow tunnel in soft ground," *Tunnelling and Underground Space Technology*, vol. 30, pp. 85–92, 2012.

[16] F. Pinto and A. J. Whittle, "Ground movements due to shallow tunnels in soft ground. I: analytical solutions," *Journal of Geotechnical and Geoenvironmental Engineering*, vol. 140, no. 4, 2014.

[17] S. R. Dindarloo and E. Siami-Irdemoosa, "Maximum surface settlement based classification of shallow tunnels in soft ground," *Tunnelling and Underground Space Technology*, vol. 49, pp. 320–327, 2015.

[18] A. Khademian, H. Abdollahipour, R. Bagherpour, and L. Faramarzi, "Model uncertainty of various settlement estimation methods in shallow tunnels excavation; case study: qom subway tunnel," *Journal of African Earth Sciences*, vol. 134, pp. 658–664, 2017.

[19] Y. Wei, W. Guo, and Q. Zhang, "A model for predicting evaporation from fresh concrete surface during the plastic stage," *Drying Technology*, vol. 37, no. 11, pp. 12–23, 2019.

[20] X. L. Yang and F. Huang, "Collapse mechanism of shallow tunnel based on nonlinear Hoek-Brown failure criterion," *Tunnelling and Underground Space Technology*, vol. 26, no. 6, pp. 686–691, 2011.

[21] I. Ocak, "A new approach for estimating the transverse surface settlement curve for twin tunnels in shallow and soft soils," *Environmental Earth Sciences*, vol. 72, no. 7, pp. 2357–2367, 2014.

[22] K. Bian, J. Liu, Z. Liu et al., "Mechanisms of large deformation in soft rock tunnels: a case study of Huangjiazhai Tunnel," *Bulletin of Engineering Geology and the Environment*, vol. 78, no. 1, pp. 431–444, 2019.

[23] A. Paternesi, H. F. Schweiger, P. Ruggeri, V. M. E. Fruzzetti, and G. Scarpelli, "Comparisons of Eurocodes design approaches for numerical analysis of shallow tunnels," *Tunnelling and Underground Space Technology*, vol. 62, pp. 115–125, 2017.

[24] X. Liu, Q. Fang, D. L. Zhang, and Y. Liu, "Energy-based prediction of volume loss ratio and plastic zone dimension of shallow tunnelling," *Computers and Geotechnics*, vol. 118, Article ID 103343, 2020.

[25] J. Fetzer, M. Holzner, M. Plötze, and G. Furrer, "Clogging of an Alpine streambed by silt-sized particles - insights from laboratory and field experiments," *Water Research*, vol. 126, pp. 60–69, 2017.

[26] S. Nazari, M. Hassanlourad, E. Chavoshi, and A. Mirzaii, "experimental investigation of unsaturated silt-sand soil permeability," *Advances in Civil Engineering*, vol. 2018, Article ID 4946956, 13 pages, 2018.

[27] M. Bryk, "Resolving compactness index of pores and solid phase elements in sandy and silt loamy soils," *Geoderma*, vol. 318, pp. 109–122, 2018.

[28] H. N. Wang, G. S. Zeng, and M. J. Jiang, "Analytical stress and displacement around non-circular tunnels in semi-infinite ground," *Applied Mathematical Modelling*, vol. 63, pp. 303–328, 2018.

[29] N. Barton, R. Lien, and J. Lunde, "Engineering classification of rock masses for the design of tunnel support," *Rock Mechanics Felsmechanik Mecanique des Roches*, vol. 6, no. 4, pp. 189–236, 1974.

[30] D. T. Niu, L. Zhang, F. Qiang, B. Wen, and D. M. Luo, "Critical conditions and life prediction of reinforcement corrosion in coral aggregate concrete," *Construction and Building Materials*, vol. 238, Article ID 117685, 2020.

[31] H. Sun, Q. P. Wang, P. Zhang, Y. J. Zhong, and X. B. Yue, "Spatiotemporal characteristics of tunnel traffic accidents in China from 2001 to present," *Advances in Civil Engineering*, vol. 2019, Article ID 4536414, 16 pages, 2019.

[32] Y. Y. Li, Y. M. Sun, J. L. Qiu, T. Liu, L. Yang, and H. D. She, "Moisture absorption characteristics and thermal insulation performance of thermal insulation materials for cold region tunnels," *Construction and Building Materials*, vol. 237, Article ID 117765, 2020.

[33] T. Liu, Y. J. Zhong, Z. H. Feng, W. Xu, and F. T. Song, "New construction technology of a shallow tunnel in boulder-cobble mixed grounds," *Advances in Civil Engineering*, vol. 2020, Article ID 5686042, 14 pages, 2020, In press.

[34] Y.-Q. Wang, Z.-F. Wang, and W.-C. Cheng, "A review on land subsidence caused by groundwater withdrawal in Xi'an, China," *Bulletin of Engineering Geology and the Environment*, vol. 78, no. 4, pp. 2851–2863, 2018.

[35] Y. Wang, S. H. Zhang, D. T. Niu, L. Su, and D. M. Luo, "Strength and chloride ion distribution brought by aggregate of basalt fiber reinforced coral aggregate concrete," *Construction and Building Materials*, vol. 234, Article ID 117390, 2020.

[36] D. C. Du, D. Dias, and X. L. Yang, "Analysis of earth pressure for shallow square tunnels in anisotropic and non-homogeneous soils," *Computers and Geotechnics*, vol. 104, pp. 226–236, 2018.

[37] Z.-F. Wang, W.-C. Cheng, and Y.-Q. Wang, "Investigation into geohazards during urbanization process of Xi'an, China," *Natural Hazards*, vol. 92, no. 3, pp. 1937–1953, 2018.

[38] M. Zhu, Y. Yang, F. Gao, and J. Liu, "Analytical solution of tunnel surrounding rock for stress and displacement based on lade-duncan criterion," *Advances in Civil Engineering*, vol. 2018, pp. 1–7, 2018.

[39] L. Bu, S. Li, S. Shi et al., "Application of the comprehensive forecast system for water-bearing structures in a karst tunnel: a case study," *Bulletin of Engineering Geology and the Environment*, vol. 78, no. 1, pp. 357–373, 2019.

[40] Y. B. Luo, J. X. Chen, W. Z. Xi, and P. Y. Zhao, "Application of a total station with RDM to monitor tunnel displacement," *Journal of Performance of Constructed Facilities*, vol. 31, no. 4, 2017.

[41] Y. Tang, K. Sun, X. Zheng, Q. Yang, and J. Zhou, "The deformation characteristics of saturated mucky clay under subway vehicle loads in Guangzhou," *Environmental Earth Sciences*, vol. 75, no. 5, 2016.

[42] G. Wei, Z. F. Yang, and L. L. Lin, "Study on surface settlement due to tunnel construction with shield in sandy silt area," *Journal of Wuhan University of Technology*, vol. 34, no. 2, pp. 93–96, 2012.

[43] V. N. Georgiannou, M. R. Coop, F. N. Altuhafi, and D. I. Lefas, "Compression and strength characteristics of two silts of low and high plasticity," *Journal of Geotechnical and Geoenvironmental Engineering*, vol. 177, 2018.

[44] Q. Yan, W. Zhang, C. Zhang, H. Chen, Y. Dai, and H. Zhou, "Back analysis of water and earth loads on shield tunnel and structure ultimate limit state assessment: a case study," *Arabian Journal for Science and Engineering*, vol. 44, no. 5, pp. 4839–4853, 2018.

[45] Y. Zhang, D. L. Zhang, Q. Fang, L. J. Xiong, L. Yu, and M. Z. Zhou, "Analytical solutions of non-Darcy seepage of grouted subsea tunnels," *Tunnelling and Underground Space Technology*, vol. 96, Article ID 103182, 2020.

[46] X. G. Yu, G. H. Xing, and Z. Q. Chang, "Flexural behavior of reinforced concrete beams strengthened with near-surface mounted 7075 aluminum alloys bars," *Journal of Building Engineering*, vol. 28, 2020.

[47] P. F. Li, H. H. Zou, F. Wang, and H. C. Xiong, "An analytical mechanism of limit support pressure on cutting face for deep tunnels in the sand," *Computers and Geotechnics*, vol. 119, Article ID 103372, 2020.

[48] C. Liu, L. Xing, H. W. Liu et al., "Numerical study of bond slip between section steel and recycled aggregate concrete with full replacement ratio," *Applied Sciences*, vol. 10, no. 3, Article ID 887, 2020.

[49] C. Cao, C. Shi, M. Lei, W. Yang, and J. Liu, "Squeezing failure of tunnels: a case study," *Tunnelling and Underground Space Technology*, vol. 77, pp. 188–203, 2018.

[50] Y. Y. Liu and H. P. Lai, "Load characteristics of tunnel lining in flooded loess strata considering loess structure," *Advances in Civil Engineering*, vol. 2019, Article ID 3731965, 13 pages, 2019.

[51] Y. Jiang, X. Zhang, and T. Taniguchi, "Quantitative condition inspection and assessment of tunnel lining," *Automation in Construction*, vol. 102, pp. 258–269, 2019.

[52] Z. J. Zhou, Y. Dong, P. Jiang, D. Han, and T. Liu, "Calculation of pile side friction by multiparameter statistical analysis," *Advances in Civil Engineering*, vol. 2019, Article ID 2638520, 2019.

[53] L. X. Wang, S. S. Xu, J. L. Qiu et al., "Automatic monitoring system in underground engineering construction: review and prospect," *Advances in Civil Engineering*, Article ID 3697253, 2020.

[54] X. L. Wang, J. X. Lai, J. L. Qiu, W. Xu, L. X. Wang, and Y. B. Luo, "Geohazards, reflection and challenges in mountain tunnel construction of China: a data collection from 2002 to

2018," *Geomatics, Natural Hazards and Risk*, vol. 11, no. 1, pp. 667–675, 2020.

[55] Z. P. Song, J. C. Mao, X. X. Tian, Y. W. Zhang, and J. B. Wang, "Optimization analysis of controlled blasting for passing through houses at close range in super-large section tunnels," *Shock and Vibration*, vol. 2019, Article ID 1941436, 16 pages, 2019.

[56] Y. Zheng, J. Xiong, T. Liu, X. Yue, and J. Qiu, "Performance of a deep excavation in Lanzhou Strong Permeable Sandy Gravel Strata," *Arabian Journal of Geosciences*, vol. 13, no. 16, p. 12, 2020.

[57] J. Hu, Y. Liu, Y. Li, and K. Yao, "Artificial ground freezing in tunnelling through aquifer soil layers: a case study in nanjing metro line 2," *KSCE Journal of Civil Engineering*, vol. 22, no. 10, pp. 4136–4142, 2018.

[58] M. Patil, D. Choudhury, P. G. Ranjith, and J. Zhao, "Behavior of shallow tunnel in soft soil under seismic conditions," *Tunnelling and Underground Space Technology*, vol. 82, pp. 30–38, 2018.

[59] Z.-D. Cui, "Effect of water-silt composite blasting on the stability of rocks surrounding a tunnel," *Bulletin of Engineering Geology and the Environment*, vol. 70, no. 4, pp. 657–664, 2011.

[60] J. L. Qiu, Y. W. Qin, Z. H. Feng, L. X. Wang, and K. Wang, "Safety risks and protection measures for the city wall during the construction and operation of Xi'an metro," *Journal of Performance of Constructed Facilities*, vol. 34, no. 1, p. 12, 2019.

[61] Q. Fang, D. Zhang, and L. N. Y. Wong, "Shallow tunnelling method (STM) for subway station construction in soft ground," *Tunnelling and Underground Space Technology*, vol. 29, pp. 10–30, 2012.

[62] M. N. Wang, Y. C. Dong, and Y. Li, "Analytical solution for Loess tunnel based on the bilinear strength criterion," *Soil Mechanics and Foundation Engineering*, vol. 57, no. 3, pp. 151–163, 2020.